

# Spectral Analysis of Nonlinearly Generated Second Harmonic Backscatter for Characterization of Human Carotid Plaque

Russell J. Fedewa  
Department of Biomedical  
Engineering  
Cleveland Clinic  
Cleveland, USA  
fedewar@ccf.org

Sheronica James  
Department of Biomedical  
Engineering  
Cleveland Clinic  
Cleveland, USA  
jamess4@ccf.org

Sean Lyden  
Department of Vascular Surgery  
Cleveland Clinic  
Cleveland, USA  
lydens@ccf.org

D. Geoffrey Vince  
Department of Biomedical  
Engineering  
Cleveland Clinic  
Cleveland, USA  
vinceg@ccf.org

**Abstract**— Plaque composition is generally unavailable for patients with carotid stenosis. The objective of this research is to develop a non-invasive approach for determining the composition of carotid plaque in order to improve risk stratification. Human carotid plaque is collected following carotid endarterectomy from 46 subjects. Serial histology is performed and the slides are matched to grayscale images created from RF data collected *in vivo* prior to surgery. Regions of homogenous tissue (F-fibrous, HNC – hemorrhagic and/or necrotic core, Ca – calcium) are determined based on histology. The corresponding RF data is processed by computing an average power spectrum over a 1.2 mm by 1.2 mm region (15 lines by 64 points) and normalized using a reference phantom with a 0.5 dB/cm-MHz attenuating phantom. An additional attenuation compensation is applied based on backscatter from healthy volunteer adventitia as a function of depth and frequency. Random forests were created using eight spectral parameters for both fundamental and harmonic bands. The out of bag error is 0.26, 0.25, and 0.23 for forests based on fundamental data, harmonic data, and combined data sets.

**Keywords**—ultrasound, carotid, atherosclerosis, spectral analysis, carotid endarterectomy, tissue characterization, harmonic imaging

## I. INTRODUCTION

Carotid plaque rupture and extra-cranial atherothrombosis are the predominant causes of cerebrovascular accidents (CVA) [1, 2]. The type of vulnerable or rupture-prone plaque most often associated with stroke and myocardial infarction is characterized by ulceration, intraplaque hemorrhage, necrotic core, and active inflammation [3], but knowledge of plaque composition is generally unavailable to clinicians considering the best course of treatment for patients with carotid stenosis. This is a greater concern for patients with diabetes since the diabetic sub-population in general presents with larger necrotic core regions

compared with non-diabetic patients for comparable stenosis [4].

Currently MRI is the only clinically available imaging modality able to provide compositional information, but MRI is unable to be a point-of-care tool for patients presenting with carotid stenosis arising from cost and availability limitations. Ultrasound contains the potential to be a point-of-care tool for obtaining compositional information regarding carotid plaque. Multiple ultrasound based approaches are being investigated to address the lack of compositional information available to clinicians in regards to carotid plaque. These include intravascular ultrasound [5], acoustic radiation force impulse (ARFI) [6], elastography combined with echogenicity and signal statistics [7], photo-acoustic measurements [8], and attenuation estimations [9]. In this work, we apply spectral analysis to the nonlinearly generated harmonic portion of the backscattered ultrasound signal to differentiate between carotid plaque tissue types. Preliminary work is shown for standard parameters extracted from normalized power spectra for both fundamental and harmonic bands.

## II. METHODS

### A. *In vivo* Ultrasonic Backscatter from Human Carotid

Two groups of subjects were recruited: normal subjects and subjects scheduled for a carotid endarterectomy (CEA). Both groups were age restricted to greater than 40 years since stenosis in younger patients is often due to other processes besides atherosclerosis. The CEA group inclusion criteria were that plaque must be located between the distal-end of the common carotid artery through the internal carotid artery including the common carotid artery bulb. Exclusion criteria were patients with prior ipsilateral carotid intervention. The normal group was defined by the absence of a past or upcoming carotid artery intervention on either side.

Each group underwent a research ultrasound exam that used either a Siemens S2000 or S3000 ultrasound system with a 9L4 probe (Siemens Medical Solutions USA, Inc., Malvern, PA). The sonographer chose sites separated by roughly 1 cm throughout the plaque. At each site location the transducer was

---

This work was supported by the Office of the Assistant Secretary of Defense and Health Affairs, through the Peer Reviewed Medical Research Program under Award No. W81XWH-16-1-0608. Opinions, interpretations, conclusions and recommendations are those of the author and are not necessarily endorsed by the Department of Defense or U.S. Army.

Ultrasound imaging system and probe loaned by Siemens Medical Solutions USA, Inc.

Research supported by AHA SDG Award 15SDG25700258

held still in a transverse orientation with respect to the carotid artery while 10 frames of RF data were collected using the Axius Direct software which records the post-beamformed RF signals prior to image processing. Following this acquisition, RF data was collected while slowly sliding the transducer along the skin and imaging the carotid artery in the transverse orientation. These cine loops were useful as backup data to the primary sites and more importantly provided the data necessary to locate the primary sites within the excised carotid plaque. For normal subjects, RF data was collected from both their right and left carotid arteries with 5 sites chosen centered on the bifurcation.

Each frame of RF data is composed of 456 lines by 2076 points digitized at 40 MHz. The ultrasound system settings were a 2 cm transmit focus, dynamic receive focus with a Hamming window, 4 cm depth, 9.00 MHz transmit setting, Tissue Harmonic Imaging enabled (pulse inversion), and mechanical index of 1.2. These settings and the TGC and overall gain were the same for all collections. The frame rate was 14 Hz in order to obtain pulse inversion data and maximize the number of lines per frame to aid the spectral averaging.

### B. Histology Matching

For the CEA subjects, the excised plaque was collected following surgical removal. A total of 46 CEA subjects were enrolled and RF data was collected from 178 sites. The excised plaque (see bottom right panel in Fig. 2 and Fig. 3) were ultrasonically imaged in saline to locate the sites from the *in vivo* ultrasound data acquisition. The plaque tissue was fixed using formalin followed by de-calcification (Cal-Rite, Richard-Allan Scientific, Kalamazoo, MI). At this point, the plaque tissue is imaged again in water to locate the *in vivo* sites and the tissue is marked to indicate the matched region. These multiple imaging sessions with plaque insure that we maintain the *in vivo* site location through the fixation and decalcification steps. The tissue is then paraffin embedded and sliced in 1 mm steps proximal to distal before and after the marked site and 0.5 mm steps within the marked region. At each of these steps, a pair of slides are prepared with differing stains: Movat pentachrome and hematoxylin & eosin.

Each stack of slides is reviewed and compared to the fundamental and harmonic grayscale *in vivo* images using the ex

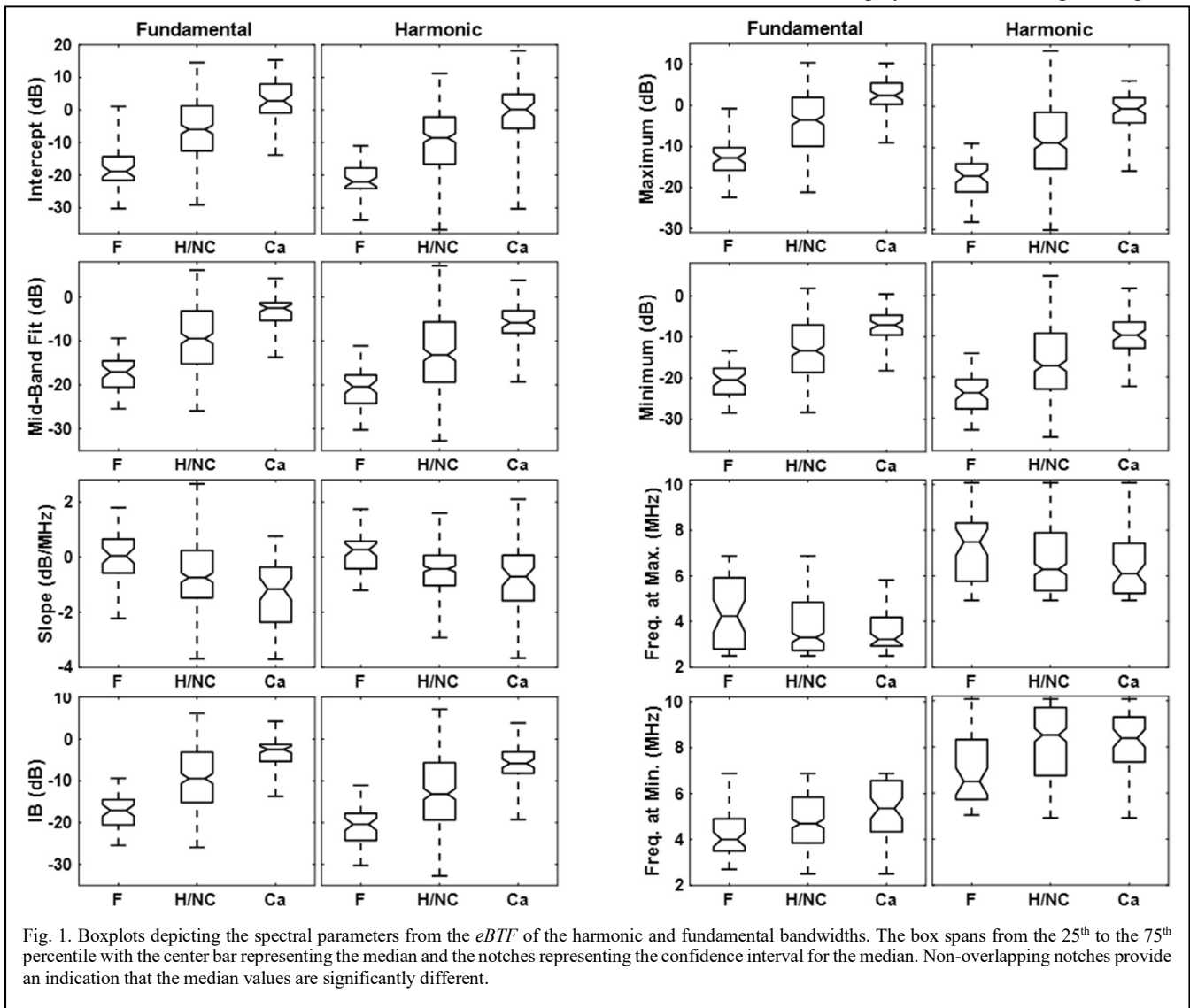


Fig. 1. Boxplots depicting the spectral parameters from the *eBTF* of the harmonic and fundamental bandwidths. The box spans from the 25<sup>th</sup> to the 75<sup>th</sup> percentile with the center bar representing the median and the notches representing the confidence interval for the median. Non-overlapping notches provide an indication that the median values are significantly different.

*in vivo* imaging data as a guide along with notes containing the relative position of the cut within the *in vivo* images. The slide that best matches the *in vivo* site is located. Then an expert in atherosclerotic plaque reads the matched slide along with the slides immediately distal and proximal to the matched slide in order to locate homogenous tissue regions. Three categories of plaque were created: F- Fibrous or Fibro-Fatty; HNC – Hemorrhagic and/or Necrotic Core with or without microcalcifications; Ca – Calcified.

This process of data collection and matching began with 178 *in vivo* sites where RF data were collected. From these sites, matches with histology were found for 86 sites (48%). Inability to match slides was due to the following: plaque not being removed, plaque sent pathology, plaque removed in pieces and thus interfering with matching, and simply low or no confidence in locating a matched histology slide to the grayscale frame. The primary reason for failure to match in roughly half the cases is that either the tissue was not provided to research or was ripped or damaged in such a manner that a match could not be reliably made. Matched sites were found for 42 of the 46 CEA subjects.

Using customized code within the Matlab environment (Mathworks, Inc., Natick, MA), regions of interest (ROI's) are

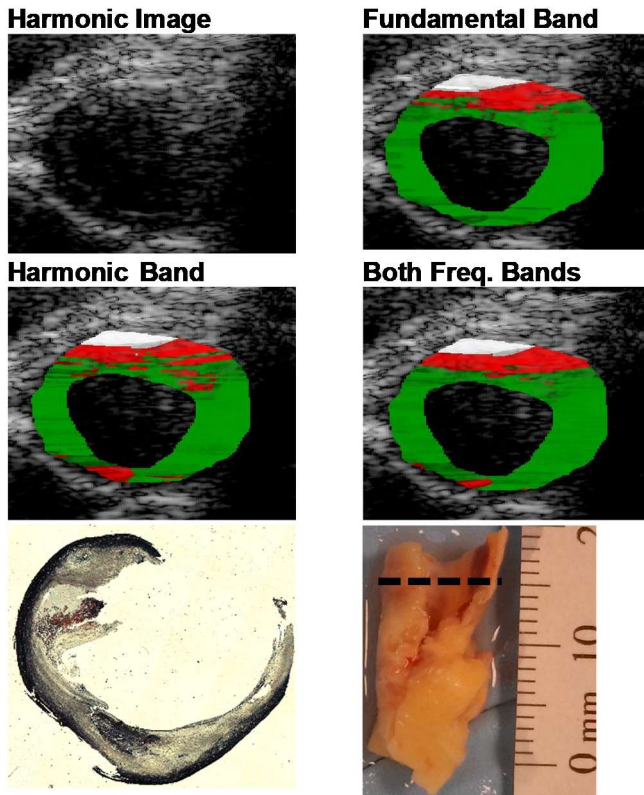


Fig. 2. Composition determined from spectral parameters for UMP0015s02 comparing the output from using parameters obtained from the Fundamental band, Harmonic band, or both frequency bands. Histology is shown in the lower left from a Movat pentachrome stain. The bottom left portion of the plaque contains a necrotic core region and the top of the plaque has calcified regions overlying a strip of hemorrhagic necrotic core with a fibrous region along the lumen however a portion of the plaque is missing on top. The bottom right image is the excised right carotid plaque with the dashed lined representing the position that matches the grayscale and histology images. Color Overlay Legend: F-Green, Ca – White, HNC – Red. Transparency level represents confidence of classifier.

defined within the RF data of 1.2 mm by 1.2 mm (64 points by 15 lines). Each ROI was placed in a region corresponding to a homogenous tissue type. A total of 378 ROI's were created with **62 Ca, 48 F, and 268 H/NC**.

### C. Signal Processing

First step in the signal processing chain was to subtract the pulse inversion signals to obtain the fundamental signal and to add them together to isolate the harmonic spectrum. An average power spectrum was obtained from each ROI for each band through use of Yule-Walker autoregressive spectral estimation approach of order 24. The -20dB bandwidths were obtained from the phantom data: 2.5 MHz to 6.9 MHz for the fundamental and 4.9 MHz to 10.1 MHz for the harmonic. These signals were normalized using a reference phantom approach (Ultrasound Phantom Model 044, Computerized Imaging Reference Systems, Inc., Norfolk, VA) [10]. In addition, the one step adventitia based attenuation compensation [11] was implemented for both harmonic and fundamental signals to obtain an estimate of the backscatter transfer function (*eBTF*).

Eight spectral parameters were extracted from the *eBTF*: integrated backscatter (IB), linear fit parameters (slope, intercept, and mid-band fit), and the minimum and maximum values along with their corresponding frequencies. These served as input parameters for three random forests based on the

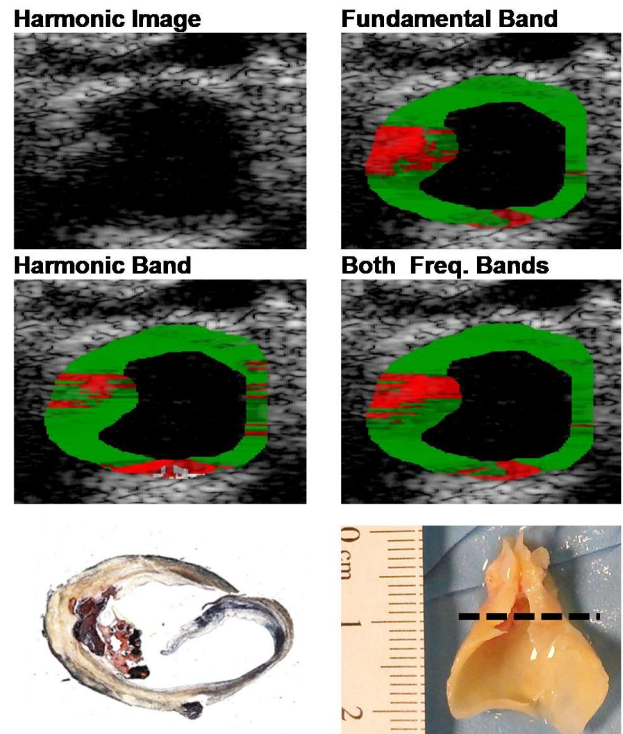


Fig. 3. Composition determined from spectral parameters for UMP0008s01 comparing the output from using parameters obtained from the Fundamental band, Harmonic band, or both frequency bands. Histology is shown in the lower left from a Movat pentachrome stain. The left side is dominated by a hemorrhagic necrotic core while the bottom nodule contains calcium. The bottom right image is the excised left carotid plaque with the dashed lined representing the position that matches the grayscale and histology images. Color Overlay Legend: F-Green, Ca – White, HNC – Red. Transparency level represents confidence of classifier.

following parameter sets: fundamental, harmonic, and both combined.

Random forests for each frequency band (and combined) were created within Matlab using 100 trees, 3 split parameters (4 for the combined), and 48 randomly chosen ROI's of each type for a balanced training set. Color overlays were produced using a 75% overlap of regions.

### III. RESULTS AND DISCUSSION

The boxplots in Fig. 1 depict the parameters obtained from the fundamental and harmonic bandwidths. At a first glance, the general trends for each parameter are comparable for both the fundamental and harmonic. The intensity-based parameters (mid-band fit, integrated backscatter, minimum, maximum, and intercept) all provide similar outcomes and trends with F corresponding to the weakest intensity and Ca corresponding to the strongest. For all of these intensity-based parameters the median values are significantly different for both fundamental and harmonic data sets.

The slope box plots in Fig. 1 depict the F category as being closest to zero and thus closest to adventitia for this measure (even though the intensity of backscatter from adventitia is closest to Ca. The H/NC and Ca are indistinguishable for the slope for both fundamental and harmonic data. Similar results are seen with the frequency corresponding to the minimum value of the *eBTF*. Results of the frequency of the maximum for the harmonic do not exhibit statistical significance for the median values though the F median value for the fundamental is significantly different. When looking at all eight spectral parameters the harmonic data does provide useful information for distinguishing between tissue types and has the potential to be beneficial for tissue characterization.

The three random forests were produced to provide a preliminary evaluation of the use of harmonic data. The out of bag error is 0.26, 0.25, and 0.23 for forests based on fundamental, harmonic, and both bandwidths combined respectively. This change in error is slight which is not surprising when seeing the example compositional color overlays in Fig. 2 and Fig. 3. Specifically, in Fig. 2, the necrotic core region on the bottom of the plaque is missed by the fundamental version of the random forest and is reasonably obtained in the harmonic version with the combined providing a smoother top region and still retaining the bottom necrotic region. Similarly, in Fig. 3, the harmonic image identifies Ca along the bottom but appears to underestimate the H/NC region on the left side where the fundamental image better represents the histology.

### IV. CONCLUSION AND LIMITATIONS

In this effort, we have applied spectral analysis for tissue characterization to the harmonic backscatter. Harmonic content demonstrates the ability to distinguish tissue types in carotid plaque and may be beneficial when combined with fundamental based input parameters. The benefits of harmonic imaging in clinical practice (reduced clutter, reduction in reverberations, improved out-of-plane mainlobe to sidelobe ratio, better resolution arising from higher frequency, etc.) are also likely to be a benefit for the use of harmonics in tissue characterization.

Limitations of this study include the following: No validation of the machine learning algorithms were performed in order to systematically compare the color overlay results with histology. No attempt was made to eliminate or weed out superfluous input parameters. Applying the reference phantom normalization approach to harmonic data is potentially flawed since the intensity of the harmonic signal has a greater dependence on the attenuation and aberration arising from the overlying tissue as compared to the fundamental band.

### ACKNOWLEDGMENT

The authors thank the skilled contributions provided by the sonographers within the Heart and Vascular Institute Vascular Laboratory at the Cleveland Clinic: Alia Grattan, Kate McDonald, Stefanie Beckner, Anyi Liu, Dmitriy Mitsyuk, Susan Whitelaw, and Tammy Rubin. Study data were collected and managed using REDCap electronic data capture tools hosted at Cleveland Clinic.

### REFERENCES

- [1] L. G. Spagnoli, A. Mauriello, G. Sangiorgi, S. Fratoni, E. Bonanno, R. S. Schwartz, D. G. Piepgras, R. Pistolesse, *et al.*, "Extracranial thrombotically active carotid plaque as a risk factor for ischemic stroke," *JAMA*, vol. 292, pp. 1845-52, Oct 20 2004.
- [2] R. C. Pasternak, M. H. Criqui, E. J. Benjamin, F. G. Fowkes, E. M. Isselbacher, P. A. McCullough, P. A. Wolf, Z. J. Zheng, and A. American Heart, "Atherosclerotic Vascular Disease Conference: Writing Group I: epidemiology," *Circulation*, vol. 109, pp. 2605-12, Jun 1 2004.
- [3] F. D. Kolodgie, K. Yahagi, H. Mori, M. E. Romero, H. H. R. Trout, A. V. Finn, and R. Virmani, "High-risk carotid plaque: lessons learned from histopathology," *Semin Vasc Surg*, vol. 30, pp. 31-43, Mar 2017.
- [4] B. B. Sun, X. Li, X. S. Liu, X. Q. Ge, Q. Lu, X. H. Zhao, J. Pu, J. R. Xu, and H. L. Zhao, "Association between carotid plaque characteristics and acute cerebral infarction determined by MRI in patients with type 2 diabetes mellitus," *Cardiovascular Diabetology*, vol. 16, Sep 11 2017.
- [5] C. M. Campos, R. J. Fedewa, H. M. Garcia-Garcia, D. G. Vince, M. P. Margolis, P. A. Lemos, G. W. Stone, P. W. Serruys, and A. Nair, "Ex vivo validation of 45 MHz intravascular ultrasound backscatter tissue characterization," *Eur Heart J Cardiovasc Imaging*, Mar 1 2015.
- [6] G. Torres, T. J. Czernuszewicz, J. W. Homeister, M. C. Caughey, B. Y. Huang, E. R. Lee, C. A. Zamora, M. A. Farber, *et al.*, "Delineation of Human Carotid Plaque Features In Vivo by Exploiting Displacement Variance," *IEEE Transactions on Ultrasonics Ferroelectrics and Frequency Control*, vol. 66, pp. 481-492, Mar 2019.
- [7] M. H. Roy-Cardinal, F. Destrempe, G. Soulez, and G. Cloutier, "Assessment of Carotid Artery Plaque Components With Machine Learning Classification Using Homodyned-K Parametric Maps and Elastograms," *IEEE Transactions on Ultrasonics Ferroelectrics and Frequency Control*, vol. 66, pp. 493-504, Mar 2019.
- [8] M. U. Arabul, H. M. Heres, M. C. M. Rutten, M. van Sambeek, F. N. van de Vosse, and R. G. P. Lopata, "Investigation on the Effect of Spatial Compounding on Photoacoustic Images of Carotid Plaques in the In Vivo Available Rotational Range," *IEEE Trans Ultrason Ferroelectr Freq Control*, vol. 65, pp. 440-447, Mar 2018.
- [9] C. Steffel, S. Wilbrand, S. Salamat, R. Dempsey, C. Mitchell, and T. Varghese, "In-Vivo Quantitative Ultrasound Evaluation of Carotid Atherosclerotic Plaque with Attenuation Coefficient," *Medical Physics*, vol. 46, pp. E491-E492, Jun 2019.
- [10] L. Yao, "Reference Phantom Method for Acoustic Backscatter Coefficient and Attenuation Coefficient Measurements," PhD, University of Wisconsin, 1990.
- [11] S. James, R. Fedewa, S. Lyden, and D. G. Vince, "Attenuation compensation comparison for human carotid plaque characterization using spectral analysis of backscattered ultrasound," in *Proceedings of IEEE IUS 2019*, Glasgow, UK, 2019.